Electronic Supplementary Material (ESI) for Journal of Materials Chemistry A.
This journal is © The Royal Society of Chemistry 2022

Supporting Information

Thiol-Functionalized Metal-organic Framework Embedded with Chelator-modified Magnetite for the High-Efficiency and Recyclable Mercury Removal in Aqueous Solution

Yuliang Li, Mengxi Tan, Guangxia Liu, Dunfeng Si, Ning Chen, Dongmei Zhou**

State Key Laboratory of Pollution Control and Resource Reuse, School of the Environment, Nanjing University, Nanjing 210023, P. R. China.

* *Corresponding author.*

Email address: chenning@nju.edu.cn (N. Chen);

dmzhou@nju.edu.cn (D. Zhou)

Number of Pages: 19

Number of Texts: 3

Number of Figures: 11

Number of Tables: 4

Text S1. Materials

All chemical agents were used as received without further purification

[1, 2]. Benzene-1,3,5-tricarboxylic acid (H_3BTC, 98.0%), $Cu(NO_3)_2 \cdot 3H_2O$(≥ 99%, AR), dithioglycol (80%, AR), 4-(5)-imidazoledithiocarboxylic acid (DTIM, 70%, CP), (3-glycidyloxypropyl)-trimethoxysilane (GLP, 97%), Fe_3O_4 nanoparticles (Fe_3O_4-NPs 98%), $Hg(NO_3)_2$ (AR) were obtained from Aladdin Reagent Co., Ltd., Shanghai, China. Toluene (≥ 99.5%, AR), thiourea (≥ 99%, AR), methanol (≥ 99.9%, GC), ethanol (75%, AR), HNO_3 (CMOS), NaOH (≥ 96.0%, AR), HCl (GR） were purchased from the Sinopharm Group Chemical Reagent Co., Ltd., China. All solutions were prepared using ultrapure water (18.2 M $\cdot cm^{-1}$) from a Synergy UV ultrapure water system with Millipak-40 filter unit (Millipore Corporation Merck KGaA, Darmstadt, Ge).

Text S2. Characterization.

The morphology and detailed microstructure of MOFs and its derivatives were examined by scanning electron microscopy (SEM, Quanta 250 FEG-SEM) and transmission electron microscopy (TEM, JEM-2100f) images equipped with energy-dispersive spectroscopy (EDS). Powder X-ray diffraction (XRD, Bruker-D8 ADVANCE) patterns were recorded on a powder diffractometer with the Cu $K\alpha$ (λ= 1.5418 Å). The spectra were scanned in the range of 10° < 2ϑ < 70° with a 0.018° step width and at 3° min^{-1}. The X-ray photoelectron spectroscopy (XPS) measurements were carried out on an ESCALAB 250Xi spectrometer (Thermo Scientific, USA) equipped with a pass energy of 30 eV with a power of 100 W (10 kV and 10 mA) and a mono-chromatized Al Kα X-ray (hv = 1486.65 eV) source. All samples were analyzed under the pressure less than 1.0×10^-9 Pa with a step of 0.05 eV. Spectra were acquired through the Avantage software (Version 5.979). Fourier transform infrared (FTIR) spectra were recorded on a Thermo Fisher Nicolet iS5 spectrometer. Magnetic properties of Fe_3O_4@DTIM-MOF@SH was measured by a vibrating sample magnetometer (VSM) (PPMS-9T Quantum Design, American) at room temperature in a magnetic field strength of 1 Tesla. The zeta potential of Fe_3O_4@DTIM-MOF@SH was recorded by Nanoscale and zeta potential analyzer (Nano ZS90). The specific surface area, pore volume and pore size distribution of Fe_3O_4@DTIM-MOF@SH samples were examined by multipoint N_2 adsorption and desorption isotherms (up to P/P_0= 1 and 77 K) by an automatic surface area and porosity analyzer (ASAP 2460, Micromeritics, America) under high vacuum in a clean system with a diaphragm pumping system.

Text S3. DFT calculation

Firstly, we use the program of GaussView to construct the cluster model (Figure S7). Then, we use Multifunctional wavefunction analyzer (Multiwfn) to generate the input file of the ORCA program for restrictive optimization with the hybrid functional PBE0 [3]. In order to examine the convergence trend of the optimization process, the OfakeG tool was used to convert the output file into a pseudo Gaussian output file, which was further processed with GaussView.

Table S1. Secific surface area/pore volume for the HKUST-1and Fe_3O_4@DTIM-MOF@SH Composites.

Sample	S_{BET}[a] (m^2 g^{-1})	V_{pore}[b] (cm g^{-1})
HKUST-1	1350	0.7013
Fe_3O_4@DTIM-MOF@SH	827	0.4058

[a] S_{BET} represents BET surface areas obtained from N_2 adsorption isotherms.

[b] V_{pore} represents pore volumes obtained from N_2 adsorption isotherms.

Table S2. Experimental values and parameters of pseudo-second-order adsorption kinetics models.

Sample	Pseudo-second-order-kinetic				
	K_1 (mg $g^{-1}min^{-1}$)	R^2	S	Fitted Q_e (mg g^{-1})	K_d
Fe_3O_4@DTIM-MOF@SH	0.29	0.99	0.009	10.31	6.2×10^5

Table S3. Isotherm model parameters for Hg^{2+} adsorption of Fe_3O_4@DTIM-MOF@SH

Sample	Langmuir isotherm				Freundlich isotherm		
	R_1^2	K_L	Fitted Q_e(mg g^{-1})	Q_e(mg g^{-1})	R_2^2	K_F	1/n
Fe_3O_4@DTIM-MOF@SH	0.995	0.023	873.4	756.9	0.968	28.06	0.653

Table S4. Comparison of various adsorbents for Hg^{2+} removal.

Adsorbent	Q_e (mg g^{-1})	K_d (mL g^{-1})	Reference
Thiol-functionalized $[Cu_3(BTC)_2]_n$	714.29	4.73×10^5	[1]
$Zn_4O(L)_3$	102.8	3.16×10^3	[4]
MOF-74	63	—	[5]
ZIF-90-SH	22.45	—	[6]
Bi-I-functionalized magnetic HKUST-1	264	—	[7]
Sulfur-functionalized MOF FJI-H12	439.8	1.86×10^6	[8]
Hydroxyl-functionalized MOF	278	—	[9]
Zr-DMBD	198.2	9.99×10^5	[10]
LMOFs	380	6.45×10^5	[11]
MIL-101-Thymine	51.27	—	[12]
Thiol-functionalized MOF	210	—	[13]
Fe_3O_4@DTIM-MOF@SH	756.9	6.2×10^5	This work

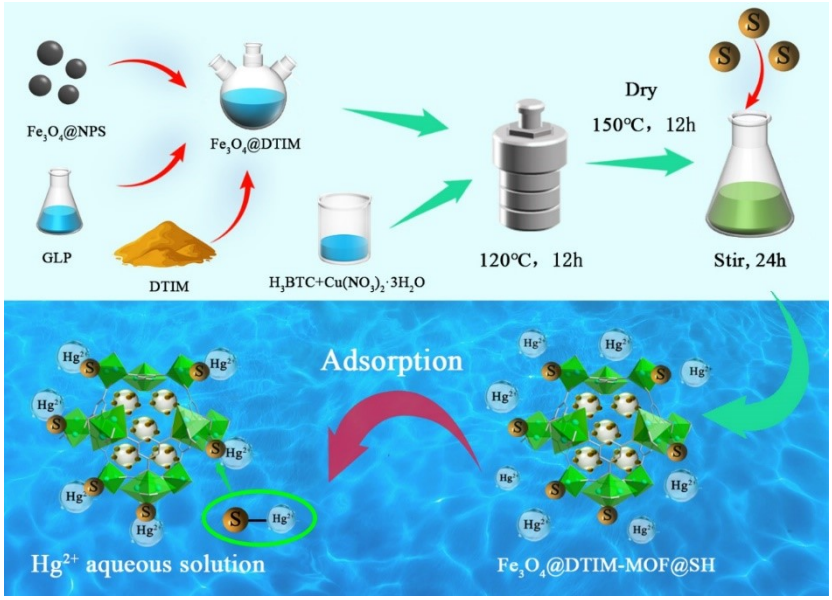

Figure S1. Schematic of preparation process of the Fe_3O_4@DTIM-MOF@SH composite.

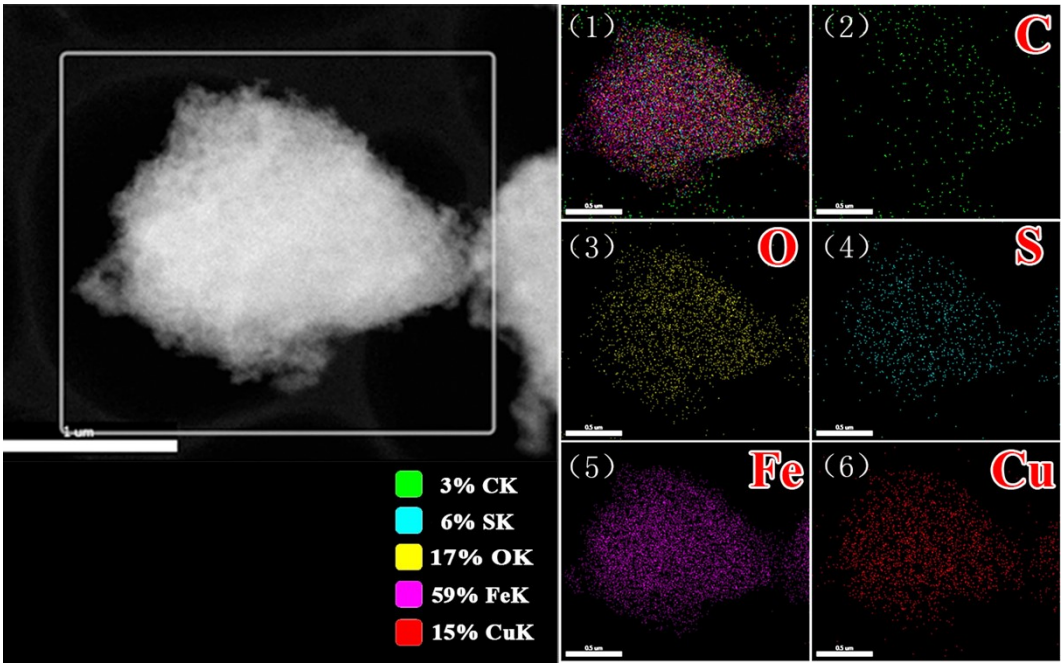

Figure S2. STEM image and EDX maps of Fe_3O_4@DTIM-MOF@SH

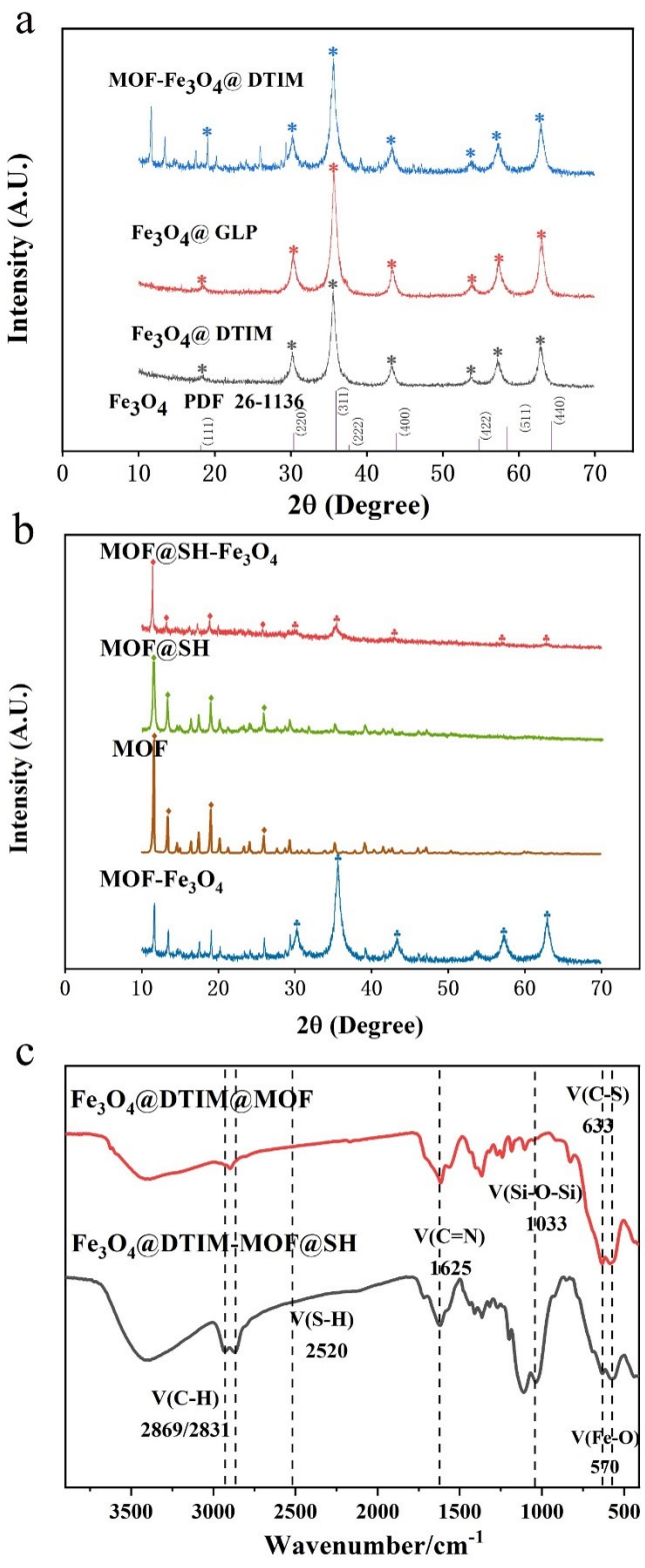

Figure S3. a) XRD partterns of as-synthesized MOF-Fe_3O_4@DTIM, Fe_3O_4@GLP, Fe_3O_4@DTIM and diffractograms of the Fe_3O_4; b) XRD partterns of MOF@SH-Fe_3O_4, MOF@SH, MOF and MOF-Fe_3O_4; c) FT-IR spectra of Fe_3O_4@DTIM-MOF and Fe_3O_4@DTIM-MOF@SH composite before adsorption.

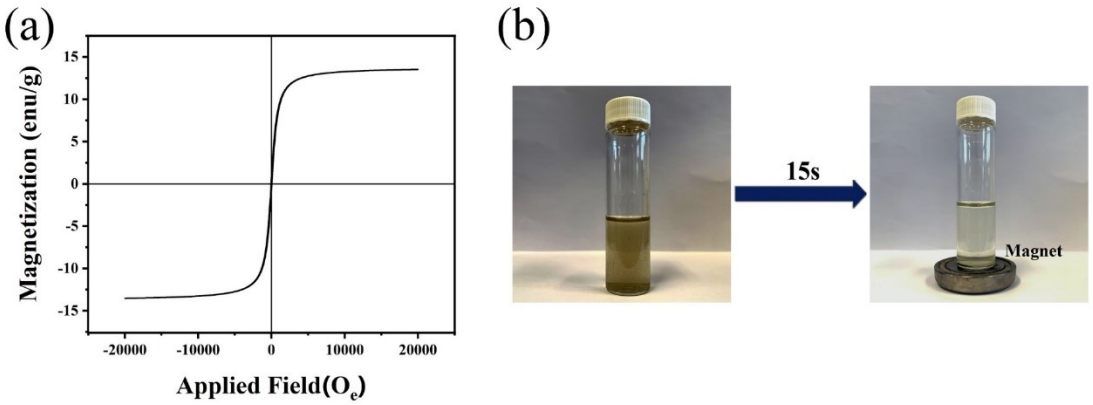

93

94 **Figure S4.** VSM analysis of Fe_3O_4@DTIM-MOF@SH and (b) magnetic separation of

95 Fe_3O_4@DTIM-MOF@SH composite.

96

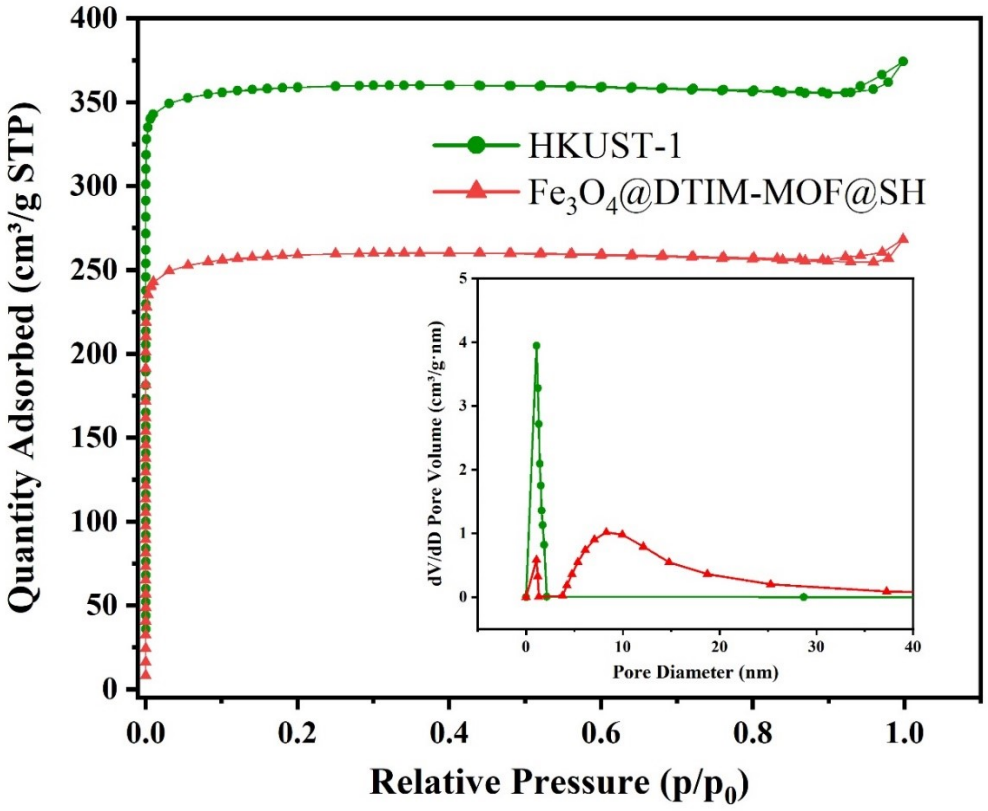

Figure S5. HKUST-1 (green) and Fe_3O_4@DTIM-MOF@SH (red) composites' N_2 adsorption isotherms at 77 K respectively; the inset shows the pore size distribution of each sample.

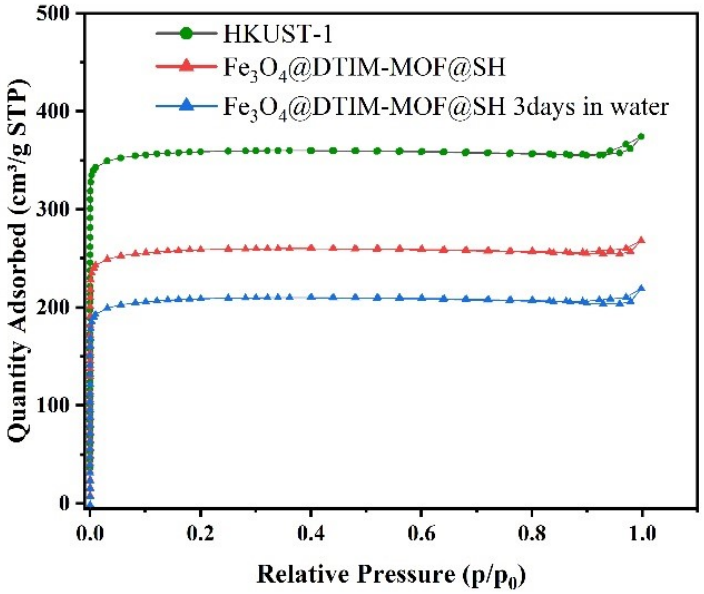

Figure S6. HKUST-1 (green) ; Fe_3O_4@DTIM-MOF@SH (red) and Fe_3O_4@DTIM-MOF@SH upon immersion in water for 3 days (blue) composites' N_2 adsorption isotherms at 77 K respectively

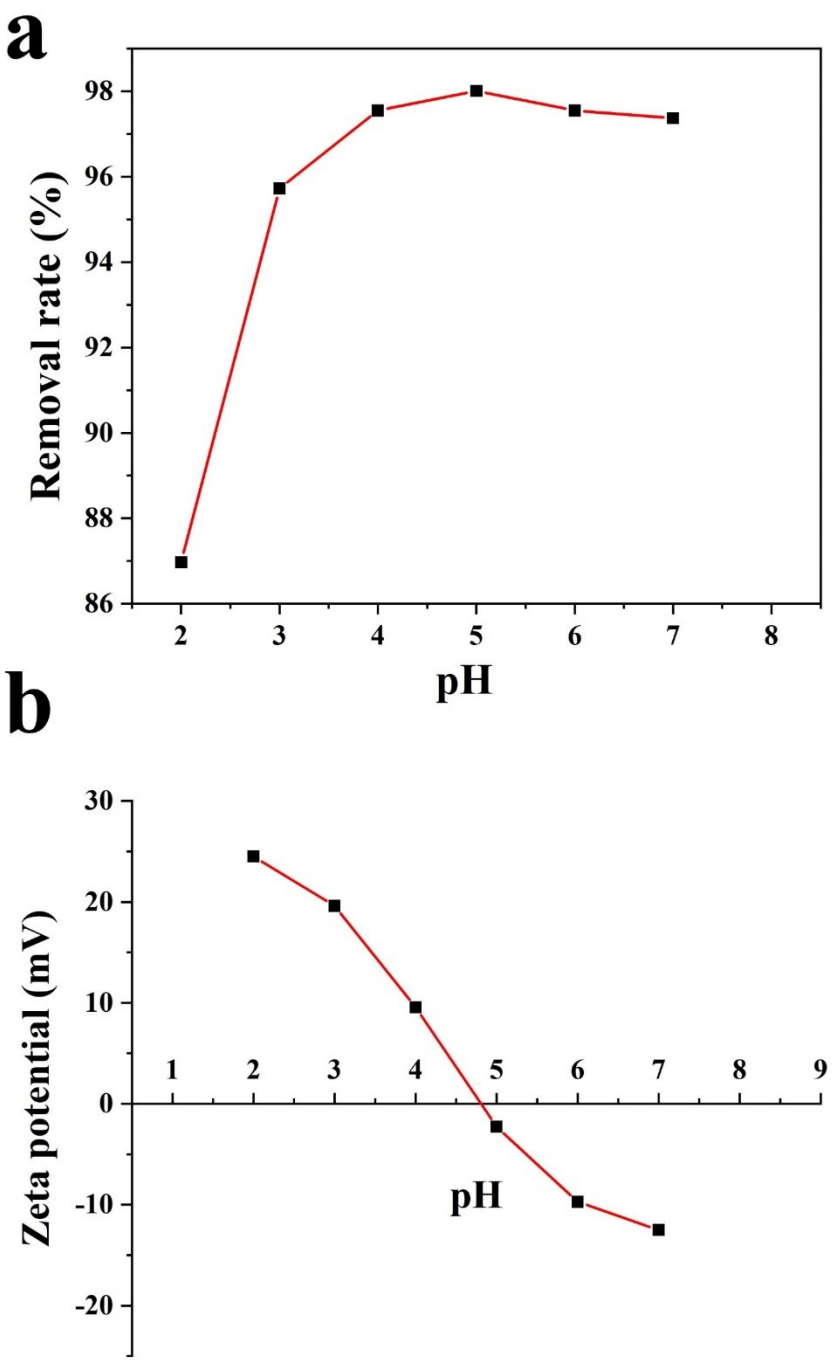

Figure S7. a) Effect of pH on the removal rate of Hg^{2+}; b) zeta potential of Fe_3O_4@DTIM-MOF@SH.

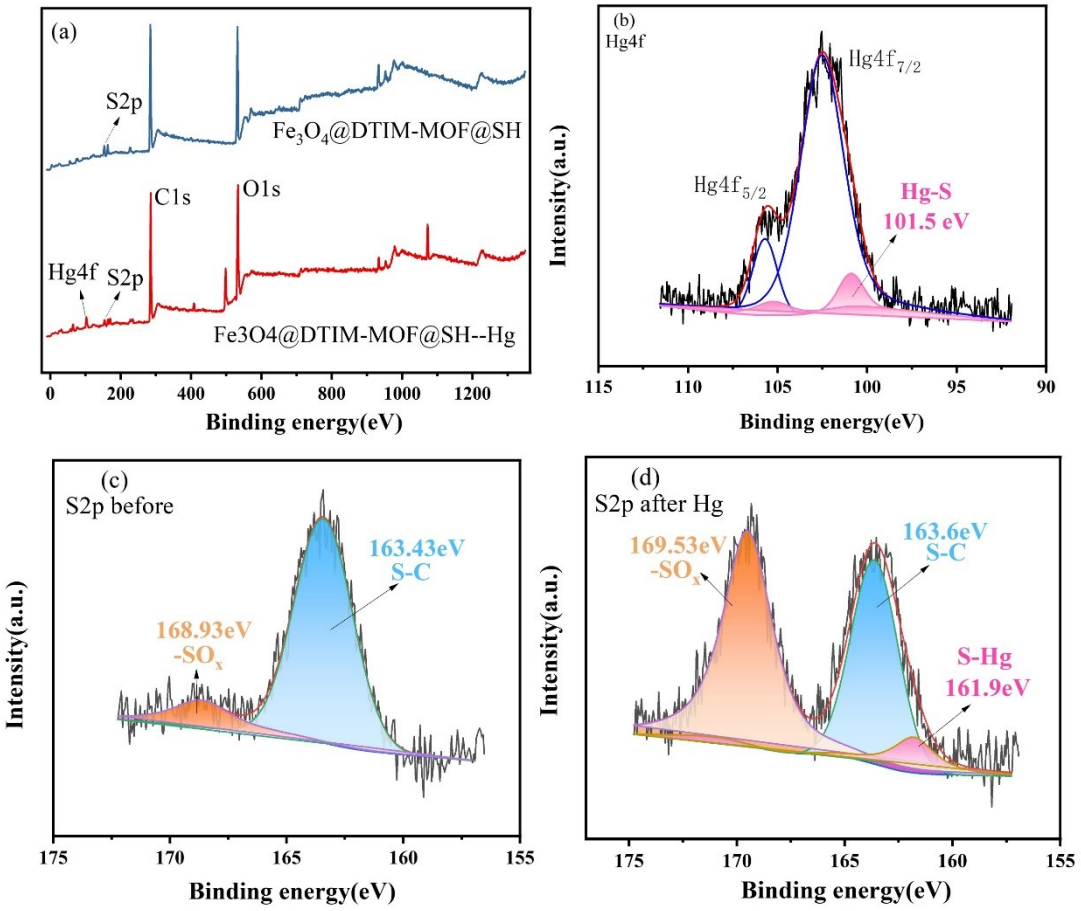

Figure S8. XPS Hg4f and S2p spectra of Fe_3O_4@DTIM-MOF@SH before and after adsorption. Area filled with blue refers to S-C, orange refers to -SO_X and pink refers to Hg-S and those binding energy are marked besides the peaks.

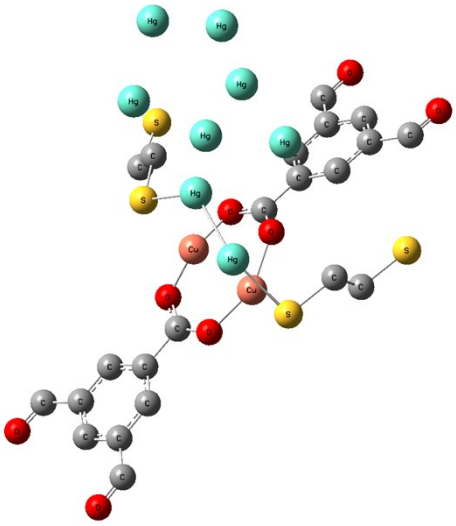

Figure S9. The cluster model of Fe_3O_4@DTIM-MOF@SH and Hg^{2+}. Atom filled with grey refers to C, green refers to Hg, red refers to O, yellow refers to S and pink refer to Cu.

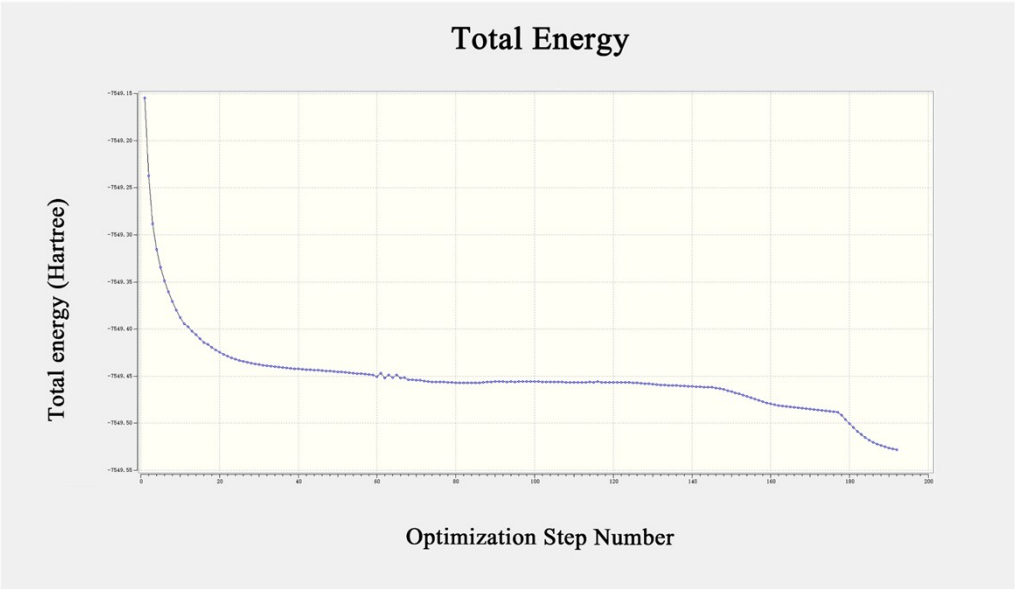

Figure S10. Energy convergence curve of the cluster model (Figure 11) after structural optimization.

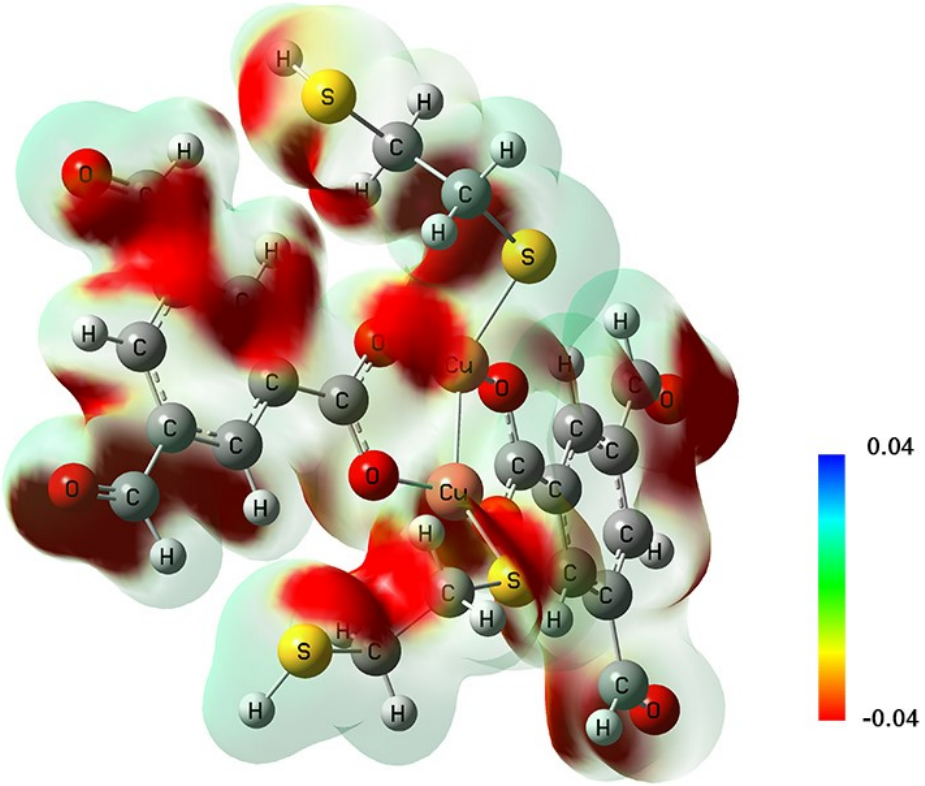

Figure S11. The electrostatic potential (ESP) population on the surface of Fe_3O_4@DTIM-MOF@SH.

References

1. F. Ke, L. G. Qiu, Y. P. Yuan, F. M. Peng, X. Jiang, A. J. Xie, Y. H. Shen and J. F. Zhu, *J Hazard Mater*, 2011, **196**, 36-43.
2. A. Tadjarodi and A. Abbaszadeh, *Microchimica Acta*, 2016, **183**, 1391-1399.
3. T. Lu and F. Chen, *J Comput Chem*, 2012, **33**, 580-592.
4. J. He, K.-K. Yee, Z. Xu, M. Zeller, A. D. Hunter, S. S.-Y. Chui and C.-M. Che, *Chemistry of Materials*, 2011, **23**, 2940-2947.
5. Y. Y. Xiong, J. Q. Li, X. F. Feng, L. N. Meng, L. Zhang, P. P. Meng, M. B. Luo and F. Luo, *Journal of Solid State Chemistry*, 2017, **246**, 16-22.
6. Z. Wang and S. M. Cohen, *Chemical Society Reviews*, 2009, **38**, 1315-1329.
7. L. Huang, M. He, B. Chen and B. Hu, *Journal of Materials Chemistry A*, 2015, **3**, 11587-11595.
8. L. Liang, Q. Chen, F. Jiang, D. Yuan, J. Qian, G. Lv, H. Xue, L. Liu, H.-L. Jiang and M. Hong, *Journal of Materials Chemistry A*, 2016, **4**, 15370-15374.
9. F. Luo, J. L. Chen, L. L. Dang, W. N. Zhou, H. L. Lin, J. Q. Li, S. J. Liu and M. B. Luo, *Journal of Materials Chemistry A*, 2015, **3**, 9616-9620.
10. K.-K. Yee, N. Reimer, J. Liu, S.-Y. Cheng, S.-M. Yiu, J. Weber, N. Stock and Z. Xu, *Journal of the American Chemical Society*, 2013, **135**, 7795-7798.
11. N. D. Rudd, H. Wang, E. M. Fuentes-Fernandez, S. J. Teat, F. Chen, G. Hall, Y. J. Chabal and J. Li, *ACS applied materials & interfaces*, 2016, **8**, 30294-30303.
12. X. Luo, T. Shen, L. Ding, W. Zhong, J. Luo and S. Luo, *Journal of Hazardous Materials*, 2016, **306**, 313-322.
13. M. R. Sohrabi, *Microchimica Acta*, 2013, **181**, 435-444.